Heat Balance of the Upper Ocean under Light Winds

JACK A. C. KAISER

Ocean Sciences Division, U.S. Naval Research Laboratory, Washington, D.C. 20375

(Manuscript received 5 August 1976, in final form 1 August 1977)

ABSTRACT

Measurements of the components of the heat balance of the upper 30 m of the ocean were made in the Bermuda area in August and September 1974. The quantities measured included surface downwelling and underwater downwelling and upwelling irradiance, surface net irradiance, heat content, and the bulk meteorological variables.

Under conditions of light winds, one or more layers of 1 to 10 m thickness form and persist at the surface. In some cases the bottom of the layers have sufficiently high Richardson numbers so that no vertical transport occurs through them, vastly simplifying the measurements and interpretation of their heat balance. These data illustrate several such cases. The net flux of heat from the layer at the surface is usually much larger than the bulk formulas predict in these light wind cases. When the winds are calm and the sea glassy, total heat fluxes of several kilowatts per square meter occur for several hours in the afternoon. This has been observed previously in the Sargasso Sea.

Generally twice during the day, the heat content of the upper ocean has an extremum, usually after sunrise and somewhat before sunset. At these times the net heat flow out of a layer is equal to the irradiance absorbed in the layer providing a simple determination of surface fluxes from irradiance measurements. These measurements show this feature clearly.

1. Introduction

Under suitable conditions measurements of the various quantities in the heat balance of the upper ocean produce valuable, and otherwise difficult to obtain, information on thermal energy transfer at the air-sea interface. Measurements of this nature have been made over a period of 50 years and reported by two dozen or so authors for both oceans and lakes. The measurements, primarily dealing with heat content of the ocean, are due to Sverdrup (1940), Stommel and Woodcock (1951), Shonting (1964), Stommel *et al.* (1969), Bowden *et al.* (1970), Delnore (1972), Kaiser and Williams (1974) and Halpern and Reed (1976). These measurements have enabled investigators to estimate the variation in air-sea heat transfer on annual and diurnal scales.

Unfortunately, in many of these studies several components of the heat balance were not measured or assumed zero with little physical justification. Notably, the horizontal heat advection was neglected, and the flux of heat and net irradiance out of the bottom of the water volume sampled were assumed negligible. Bowden *et al.* (1970) did measure the horizontal advection with a drogue, while Stommel *et al.* (1969) surveyed their area to find a homogeneous water mass and then drifted, which approximated a Lagrangian reference frame. Kaiser and Williams (1974) avoided the question of irradiance through the bottom of the volume by making measurements only at night.

In this study, horizontal advection of heat and the vertical transport of heat and downwelling irradiance through the bottom of the control volume are either measured or special precautions are taken to make them small in the heat balance measurements. The data sets used here were obtained under light wind conditions; thus shallow layers bounded below by sharp interfaces were present throughout the majority of the measurement periods. In these cases the flux of heat through this interface by convection and turbulent mixing is zero, and the residual conductive flux is small compared to that through the air-sea interface. This is shown by a Richardson number argument, by the measurements of the heat budget of the layer below the surface layer, and by the fact that the mean depth of the mixed layer below the surface does not change with time.

Because of the shallow layer formation, and because the measurements were made well away from the regions of strong surface currents or horizontal temperature gradients, the net horizontal advection of heat in these surface layers relative to the flux out of the layer is bounded by a negligibly small value, i.e., the maximum value it *could* have based on measurements in the area is negligibly small. This is seen from the fact

that the net horizontal advection in a layer is proportional to the layer thickness. The downwelling and upwelling irradiance through the bottom of the control volume were determined from irradiance measurements made in the water during the duration of the heat balance measurements.

The existence of shallow surface layers is very helpful in eliminating contamination of the data due to horizontal anomalies which introduce enough noise into the time series of temperature taken from a slowly moving ship to seriously mask the variations solely due to heating. This is demonstrated in Section 4.

The quantity of prime interest in these measurements is the heat transfer between the sea and the atmosphere, both from the standpoint of atmospheric forcing and determination of the skin temperature of the sea. Several other techniques exist for heat transfer measurement—the eddy correlation method, the dissipation method and the bulk formulas method; but the heat content method is inherently simple and as such deserves further exploration.

The measurements discussed here were made from the USNS *Lynch* in August-September 1974 in the Sargasso Sea at 34°N, 71°W and 32°N, 65°W. Five data sets were obtained, of which three showed enough surface layering to be able to justifiably equate the heat loss from the mixed layer above the interface with the total surface heat flux.

2. Formulation

The temperature profile in an ocean with a mixed surface layer and a deeper seasonal or secondary mixed layer would appear as shown on the left of Fig. 1. The downwelling irradiance just above the ocean surface is $Is\downarrow$ (W m^{-2}) and the surface transmissivity for total downwelling irradiance is τ; $Is\uparrow$ is the surface upwelling irradiance; and $Ii,u\downarrow$ and $Ii,u\uparrow$ are upwelling and downwelling irradiances at the bottom of the ith layer. The horizontal or advective heat transfers h_i, h'_i (W m^{-2}) are, respectively, the inward and outward fluxes on the sides of the ith layer. Here the ocean is treated as two-dimensional. The downward flux from layer i to $i+1$ is $h_{i,d}$; the upward flux into layer i from $i+1$ is $h_{i,u}$; hence $h_{i,d} \equiv -h_{i,u}$, and H_i is the heat storage or content term of the ith layer:

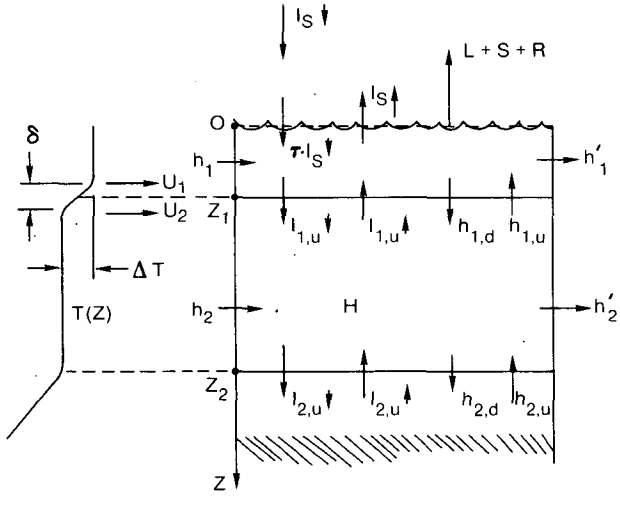

FIG. 1. Schematic of the upper ocean showing the expected temperature structure with layer formation and the various irradiative, advective and surface fluxes making up the heat budget.

$$H_i = \int_{z_i}^{z_{i+1}} \rho c_p [T(z) - T_B] dz, \tag{1}$$

where ρ is the density (g m^{-3}), c_p the specific heat (J kg^{-1} °C^{-1}), $T(z)$ the temperature, and T_B a temperature which is independent of z and is chosen as a reference temperature.

For the ith layer an integration of the thermodynamic equation over the layer depth yields, neglecting chemical reactions and mechanical-thermal conversions,

$$\frac{\partial}{\partial t} H_i + h_i - h'_i - h_{i,u} + h_{i+1,d} = I_{i,u}\downarrow - I_{i,u}\uparrow - (I_{i+1,u}\downarrow - I_{i+1,u}\uparrow), \tag{2}$$

where t is time. Note that the various h's represent total fluxes; these include conduction, convection, advection and turbulent mixing. If we sum (2) for adjacent layers, all interfacial terms cancel leaving only fluxes through the top, bottom and sides.

For the surface layer ($i = 1$),

$$\left.\begin{aligned} h_{i,u} &= L + S + R \\ I_{i,u}\downarrow &= \tau \cdot Is\downarrow \end{aligned}\right\}, \tag{3}$$

where L is the evaporative or latent heat flux, S the sensible heat flux and R represents the net longwave radiation emitted by the sea at the surface.

Since we intend to look at the existence of stable interfaces between mixed layers as illustrated in Fig. 1, it is useful to define a Richardson number Ri as

$$\mathrm{Ri} = \frac{\partial \rho / \partial z}{\rho (\partial U / \partial z)^2} = \frac{g \epsilon \Delta T \delta}{(U_2 - U_1)^2} = \frac{N^2}{\delta^2}, \tag{4}$$

where g is gravity, ϵ the thermal expansion coefficient of water, ΔT the temperature difference across the interface, δ the thickness of the layer, $(U_2 - U_1)$ the velocity difference across the interface and N the Brunt-Vaisälä frequency. The layers under consideration are only a day or so old and have no salinity difference across them; hence the temperature difference is adequate

to represent density differences in (4). The salinity was measured and bears this out.

3. Irradiance measurements

To determine the radiative energy input to a surface layer, the downwelling irradiance just above the surface, the surface transmittance, the downwelling irradiance at the bottom of the layer and the upwelling irradiance field are necessary.

a. Surface downwelling irradiance

Total downwelling irradiance was measured with an Eppley 8-48 black and white pyranometer mounted about 5 m above the sea surface. These instruments have a flat response over the 0.28–2.8 μm band; this includes over 98% of the global irradiance. The instrument was not gimballed; however only at low solar elevations could an oscillation due to ship roll be noted on the pyranometer signal; however, using the average of this signal introduces an error which is less than 0.4%. This difference is within instrument error so a gimballed mount was not necessary under these conditions. The pyranometer has a time constant of about 4 s. The output was fed directly into a strip chart recorder, and visual integrations over 15 min intervals were used for $Is\downarrow$.

b. Surface transmittance

The transmittance τ at the air-sea interface is complicated by the presence of waves which have a significant effect on the direct solar beam. Payne (1972) found from extensive albedo measurements over water that τ could be accurately determined from the atmospheric transmissivity which is in turn calculated from $Is\downarrow$. Payne's empirical relations are used here to determine τ.

c. Underwater irradiance

To determine the downwelling and upwelling irradiance at the bottom of a layer, the underwater measurements were made throughout the period at a depth of 5 m with pyranometers and then corrected to the layer depth using underwater irradiance data cited in Jerlov (1968).

Two pyranometers (uplooking and downlooking) were mounted on a "sled" which was towed 100 m behind the ship. The sled was configured to maintain a nearly level platform for the pyranometers. This was verified by two mutually orthogonal pendulum inclinometers. The depth of the instruments was continually monitored. The sled pitched and rolled with a period of the order of a few seconds but was always aligned within 3° of horizontal.

The pyranometers had glass hemispherical domes over the sensing elements. As a light ray enters from the water to glass to the air between the dome and the element, it undergoes a strong refraction and the glass dome acts like a concave lens diverging the light field and reducing the sensitivity of the instrument by about 45%. Careful calibrations to correct for this were done in the laboratory. Also the underwater cosine response of the pyranometer was verified. Details of the sled configuration, behavior and pyranometer calibrations are given in Kaiser (1976).

Since the sled was towed 100 m behind the ship, a negligible portion of the field of view of the upper instrument was occluded by the ship. The sled was supported by several members at the surface, but in total, 0.4% of the Snell circle of the upper pyranometer was obscured.

Overall, the probable error of the underwater downwelling irradiance $Iu\downarrow$ was about 3% of which 1% was due to cosine response errors, 1% to calibration error, and the rest to obscuration and other factors. The upwelling irradiance $Iu\uparrow$ error was considerably larger and is not accurately known, but it is believed to be about 10%.

Determinations of $Iu\downarrow$ and $Iu\uparrow$ were made every half-hour during daylight and twilight and from these the ratios $r_1 = Iu\downarrow/Is\downarrow$ and $r_2 = Iu\uparrow/Is\downarrow$ were calculated. Then the half-hourly averages of $Iu\downarrow$ and $Iu\uparrow$ at 5 m were taken as

$$\overline{Iu\downarrow} = r_1\overline{Is\downarrow}, \quad \overline{Iu\uparrow} = r_2\overline{Is\downarrow}. \tag{5}$$

The sled depth was 5 ± 0.05 m for all determinations.

To determine $Iu\downarrow$ at the bottom of the layer when it was other than the 5 m depth of the sled, data given by Jerlov (1968) on the depletion of total irradiance from the sun and sky are used. Jerlov classifies oceanic water as type I, IA, IB, II or III according to its optical clarity, type I being the clearest. Curves from Jerlov data are plotted in Fig. 2. These curves represent a clear sky with a solar zenith angle of 0°. The vertical bar shows the range of our measurements at 5 m. The double bar is for clear skies and has the maximum value of 0.33. This compares to Jerlov's value of 0.30 for type I water. Thus,

$$Iu\downarrow(z) = Iu\downarrow(5)\left[\frac{Iu\downarrow(z)/Is\downarrow}{Iu\downarrow(5)/Is\downarrow}\right], \tag{6}$$

where the ratio in the brackets is taken from Jerlov's type I curve and $Iu\downarrow(5)$ from our determinations.

d. Absorbed radiation

Throughout the data at 5 m, $r_2 = 0.04$, a value independent of depth to first order away from the

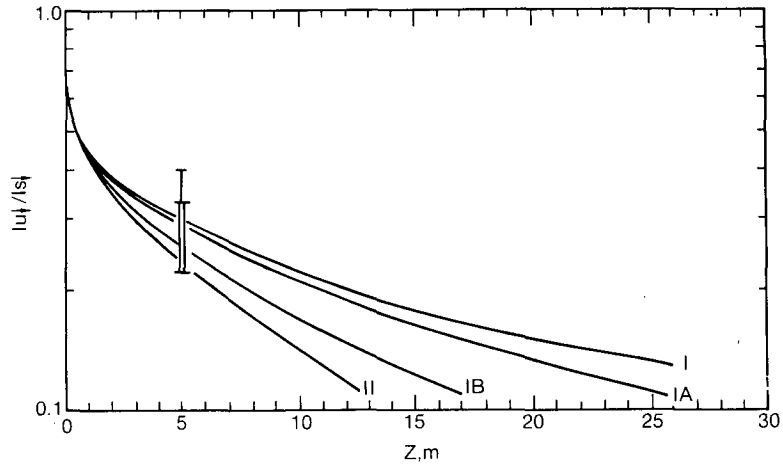

FIG. 2. The depletion of global irradiance for a solar zenith angle of 0° for water mass types I, IA, IB and II according to Jerlov's (1968) classification. The vertical bar at 5 m is the range of all of our underwater measurements at 5 m. The double bar is the range for clear skies only, and the top of this bar is for the smallest solar zenith angle (22°).

surface (Jerlov, 1968). The upwelling irradiance $Is\uparrow$ just below the sea surface was not measured, but Jerlov gives 0.012 for $Is\uparrow$ for the Sargasso Sea. Thus the total heating by radiation, the right-hand side of (2), is

$$I_{\text{abs}} = Is\downarrow[0.988\tau - r_1(z)(1 - r_2)] \qquad (7)$$

for a layer from the surface to a depth z. The correction for upwelling irradiance is very small (<1%).

4. Heat content

a. Measurement

The heat content of the water column was derived from temperature profiles taken at specified intervals not greater than 30 min. A calibrated thermistor was used in conjunction with a bellows-type pressure transducer. The thermistor had 50 mV across it, which produced less than 0.0005°C temperature rise in still water. Conductivity of the water was also determined with a Beckman RS5-3 portable salinometer modified to operate remotely from a shipboard stabilized voltage supply.

The sensor outputs were displayed on an x-y plotter and subsequently read by hand. The temperature and conductivity were averaged over depth intervals of 0.8 m in the upper 17 m and over 1.8 m intervals below 17 m. The temperature sensitivity was 0.014°C mm^{-1} of chart and was read to the nearest 0.1 mm. The typical conductivity sensitivity was 0.024 mm cm^{-1} per millimeter of chart which corresponds to a salinity sensitivity of 0.016 per millimeter of chart.

The air temperature was determined with a calibrated thermistor mounted at 10 m on a boom slightly forward of the bow. The dewpoint was measured with a Cambridge Systems 137-C1 thermoelectric dewpoint hygrometer system. The sea surface temperature was taken from our profile data and represents an average over the upper 0.78 m of the water column. Net radiation was monitored continuously with a Fritschen net radiometer mounted on the boom forward of the bow.

b. Data reduction

One typical set of temperature data is displayed in profile form in Fig. 7a. Each point represents an average over the depth interval specified above. In Fig. 3 the same set of raw temperature data is plotted as a time series for the upper 26 intervals. Each curve is displaced upward from the one below by the equivalent of 0.02°C (the temperature axis is for the lowest curve). One of the prominent features of the temperature structure is large, vertically coherent fluctuations throughout the upper 25 m of nearly 0.3°C over time scales of several hours. Since the ship made way between casts, these fluctuations probably represent spatial anomalies of 5–10 km.

The heat content of the water column between the surface and depth z' with respect to a reference temperature T_B is

$$H_0 = \int_0^{z'} \rho c_p[T(z) - T_B]dz. \qquad (8)$$

If we choose T_B as a constant temperature, H_0 calculated from the data of Fig. 3 would have short-term fluctuations in some cases greater than the diurnal variation of interest here as the broken curve of Fig. 4 shows.

Because of the high vertical thermal coherence

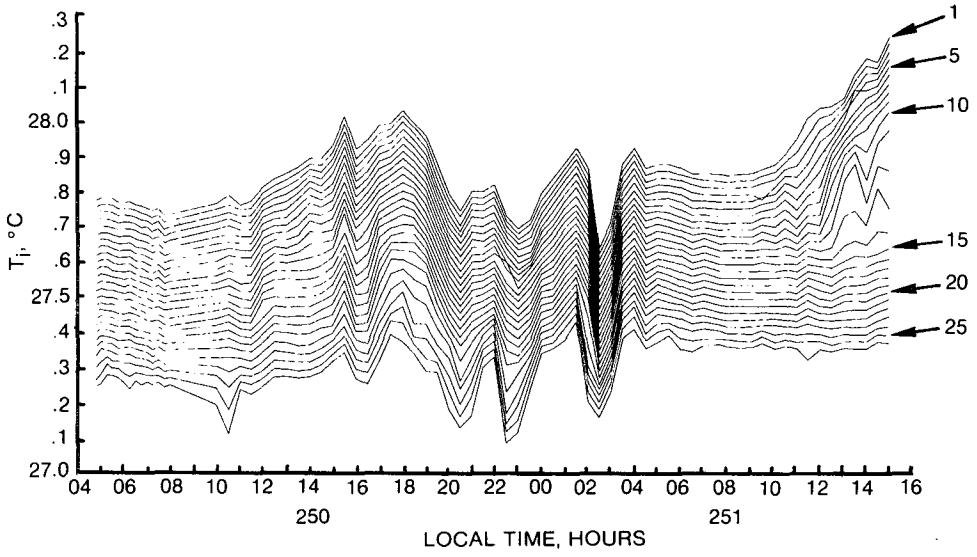

FIG. 3. Temperatures at 26 depths throughout the measurement period of set B. The upper 20 curves represent temperatures averaged over every 0.80 m slab and the lower 6 curves over every 1.9 m slab. The total depth covered is 27.5 m. Each curve is displaced upward the equivalent of 0.019°C from the one below. The temperature scale is for the lowest curve. Note the high vertical coherence in the mixed layer except for the pronounced heating of the upper 13 layers at the end of the data set.

of the mixed layer displayed by these data, one can remove the largest portion of these short-term variations by choosing T_B as the temperature of a level deep enough so that it is negligibly affected by diurnal heating. The choice of T_B being the average of $T(z)$ from 15.5 to 21.5 m produces the broken curve of H_0 shown in Fig. 4b. Now the afternoon heating is much more discernible than for the constant T_B, and only two sharp peaks occur around 0000 local time 8 September.

There is good physical reason for this procedure. As the upper ocean cools at night, convection transfers heat vertically in the water. As this convection penetrates more deeply, it removes any vertical temperature structure so that just after sunrise any temperature structure in the water is essentially two-dimensional (horizontal) and can be represented by $T_1(x,y)$. During the following day, when light winds prevail and a shallow, mixed layer forms just below the surface, the temperature field in this layer can be represented by

$$T(x,y,t) = T_1(x,y) + T_2(t), \qquad (9)$$

where the $T_2(t)$ is due only to heating. The level of T_1 must be deep enough so that is affected only very little by solar heating, and the presence of a stable interface at the bottom of the mixed layer and above the reference depth is necessary to ensure that there are no vertical advective heat transfers. If mixing were not complete near the surface, T_2 would also be a function of z and then so would T.

This mechanism is evident in the casts of Fig. 7a. A layer interface between 10 and 15 m is apparent in the temperature field in the afternoon of day 250. Throughout the night the water column gradually

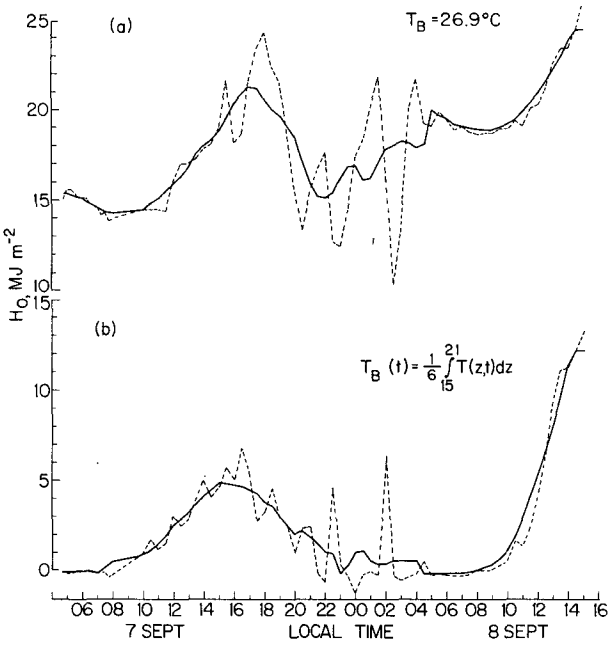

FIG. 4. The heat content of the upper 26.55 m of the ocean for data set B determined by several different techniques using Eq. (8). The broken curves are from the actual data while the solid curves are smoothed with a 4 h running boxcar filter. (a) is for a reference temperature of 26.9°C and (b) for a reference temperature which is an average from 15 to 21 m depth. The latter removed some large heat content anomalies.

becomes isothermal down to 30 m, the top of the seasonal thermocline. Then as heating increases during day 251, its thermal signature is superimposed on $T_1(x,y)$.

In the data reduction, the diurnal variation of T_B due to solar heating was neglected and this produces an *underestimate* of H_0. In Table 1, heating rates for two adjacent uniformly mixed layers having an interface between them at z and a total thickness of 20 m are given in columns two and three based on Jerlov's (1968) data for type I ocean water when the total downwelling irradiance is 20.95 MJ m^{-2} day^{-1}. The second column represents the daily temperature rise for a well mixed layer from the surface to depth z due to irradiative heating and the third column is the daily warming of a lower layer from z to 20 m, i.e., T_B. The error in H_0 due to the neglect of the diurnal variation in T_B for surface layers of various depths is given in the last column. For a 5 m thick layer it is about 7%.

If the measuring platform could drift with the near-surface waters, the use of T_B may not be necessary; but making way, the ship cut through these inhomogeneities. This procedure replaces a mapping of the horizontal temperature inhomogeneities in the area before making measurements and then correcting them for the horizontal structure. It also averages heat fluxes over the experimental area.

The heat contents resulting from this correction procedure are still quite noisy as Fig. 4 shows, and temporal smoothing would seem to be warranted. Much of the data indicate a periodicity in the noise of about 4 h. A 4 h running boxcar filter was used to suppress this. The results of the use of such a filter on H_0 is shown in Fig. 4 as the solid curves. Then the diurnal heating becomes quite discernible. The solid curve of Fig. 4b, which is the result of a combination of filtering and correction by the use of T_B from below the mixed layer then represents the temporal heat content variation under light winds and strong insolation in a horizontally homogeneous ocean.

TABLE 1. Radiative heating of the ocean*

Z (m)	ΔT (°C day^{-1}) 0–z	z–20	Error (percent)
0.1	17.15	0.13	0.8
0.5	4.70	0.095	2.0
1.0	2.55	0.087	3.4
2.0	1.50	0.066	4.4
3.0	1.06	0.059	5.6
4.0	0.83	0.053	6.4
5.0	0.70	0.047	6.7
7.5	0.49	0.040	8.2
10.0	0.38	0.035	9.2
15.0	0.26	0.030	11.5
20.0	0.21	—	—
30.0	0.15	—	—

* 20.95 MJ m^{-2} day^{-1} (500 ly day^{-1}) total absorbed.

c. *Horizontal advection*

Because of the presence of shallow layers and because the measurements were taken near the middle of the Atlantic Gyre, the contribution to the heat budget by horizontal heat transport in the region under consideration is negligible; this is demonstrated below. For a layer of depth D, mean horizontal velocity U, and horizontal temperature gradient in the direction of U of ∇T, the net horizontal heat gain per square centimeter of surface area is

$$h_h = h_i - h_i' = \rho c_p U D \nabla T. \tag{10}$$

From charts of the surface temperature in the Atlantic for August and September 1974 (U.S. Naval Oceanographic Office, 1974) $\nabla T = 10^{-8}$°C cm^{-1}. For a layer of depth 5 m and a surface current of 50 cm s^{-1} (1 kt), $h_h = 10.5$ W m^{-2}, which for most cases is negligible. The major factors which cause h_h to be small are the weak currents and the small layer depth. For a 50 m layer (for a typical depth of the top of the main thermocline) $h_h = 105$ W m^{-2}, which is not negligible.

Here a relatively large value of U was chosen. Using the Naval Oceanographic Office ship drift file, Wyrtki *et al.* (1976) estimated for 30°N a mean current of 10 cm s^{-1} and an eddy component of 25 cm s^{-1}; these values are on the average typical of the world oceans. A value of 50 cm s^{-1} for U was obtained from the *Oceanographic Atlas of the North Atlantic Ocean* (1965) for the area and season in which these measurements were made.

5. Heat budgets

In August–September 1974 the heat budget components were determined for five different periods ranging from 12 to 36 h. Of these, three data sets exhibited sufficient layering so that this analysis could be carried out. The earliest of the five (set C) showed very pronounced layering. The third (set A) showed a double layer structure, the shallower of which was quite pronounced and the fifth (set B) showed less pronounced and more intermittent layering than the others. Of the two data sets not exhibiting layering, the second was under moderate winds (5–10 m s^{-1}) and weak insolation; hence surface heating was not pronounced. The fourth was at night under moderate winds. The latter showed a total cooling of the upper ocean of 265 W m^{-2}, while 202 W m^{-2} was the average rate determined using the formulas

proposed by Friehe and Schmidt (1976) in their summary of reliable sensible and latent fluxes measured by various investigators. The important consideration here is that in the subtropical oceans during the summer and fall months, light wind and strong insolation occur frequently enough so that the use of layering as an aid in heat budget analyses is of significant applicability.

The series of temperature profiles from set A is shown in Fig. 5a. They start at 1400 (all time is local time) and cover a 24 h period. Sunrise was about 0630 and sunset was 1915. A surface (upper) layer is apparent throughout the period which appears variable in depth between 3 and 9 m (layer 1) and in the mean the layer neither deepened nor becomes more shallow. The mean layer depth was taken as 7.14 m. A lower layer, down to the seasonal thermocline, has its bottom at a mean depth of about 27 m (layer 2). For our heat budget determinations the bottom of the second layer was taken as 16.7 m to remove as much variability in heat content as is possible (16.7 m is the greatest depth not affected by internal waves). A very shallow third layer started to form late in the afternoon of the second day.

The variation of the heat content for the several layers is given in Fig. 5b for the period. The top three data point sets are the time-integrated heat losses H_i^* from depth z to the surface for each of the three layers, i.e.,

$$H_i^* = \int_{t_0}^{t} I_{i,a}dt - H_i, \tag{11}$$

where $I_{i,a}$ is the irradiance absorbed between 0 and z, and the corresponding heat content H_i is the filtered value. The origin is shifted vertically for each curve as indicated. The initial time t_0 is taken from the start of measurement. The slope of each of these curves is the *total* heat flux out of the water column above the indicated level. The solid curve $H_1 + H_2$ is the total heat content of

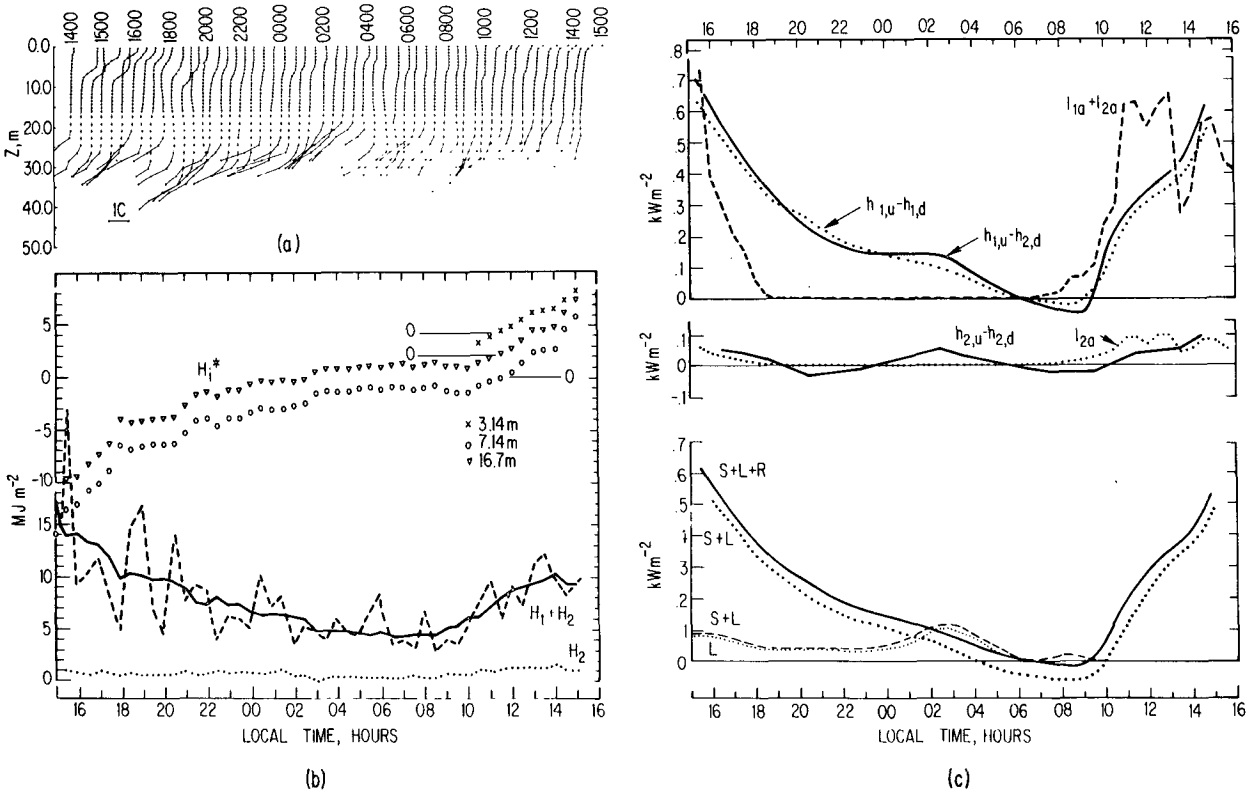

FIG. 5a. The set of temperature profiles for data set A. The local times of several of the profiles are indicated near the top. A quasi-persistent mixed layer appears above 7 m throughout the period with a pronounced mixed layer above 3 m appearing at the end of the period. 5b. The time integrated heat content H_i^* from the surface down to the various interfaces between the mixed layers indicated by their depths. Layer 1 extends from 0–7.14 m, layer 2 from 7.14–16.7 m and layer 3 from 0–3.14 m. The heat content of the top two layers is $H_1 + H_2$; the solid line is smoothed. H_2 is the heat content of layer 2. 5c. The various components of the heat balances of the several layers which occur during A. I is the absorbed radiation, $h_{i,u}$ the upward flux of heat from the ith layer, and $h_{i,d}$ the downward flux of heat from the ith layer. The total surface flux $S + L + R$ and the total less the infrared radiation $S + L$ (heavy lines) are determined from the heat balance, and $S + L$ and the latent heat flux L (faint lines) are determined from Friehe and Schmidt (1976).

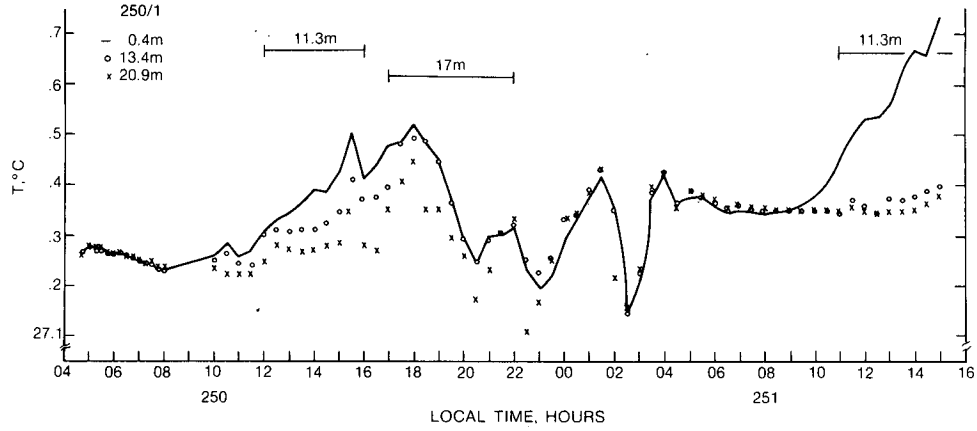

FIG. 6. Temperatures from data set B at 0.4 m (surface), 13.4 m and 20.9 m. The depths and times at which layers are discernible on the profiles are shown above the curves. Even though Fig. 7a does not indicate strong layering, there is still a stable temperature gradient throughout the upper 20 m up to 2100 on 7 September; it again appears at 1000 on 8 September.

the top two layers (0–16.7 m) and H_2 the heat content of the lower layer (7.14–16.7 m). The broken curve is the heat content from the raw data and the solid curve is the smoothed value for the two layers.

The components of the heat balance are given in Fig. 5c. The solid curve $h_{i,u} - h_{2d}$ is the smoothed slope of the H_i^* data for 0 to 16.7 m, and this is the total flux of heat of the upper two layers. The dashed curve $h_{1,u} - h_{1,d}$ is the smoothed heat flux from the upper layer and is the slope of H_i^* for 7.14 m. The broken curve $I_{1a} + I_{2a}$ is the total

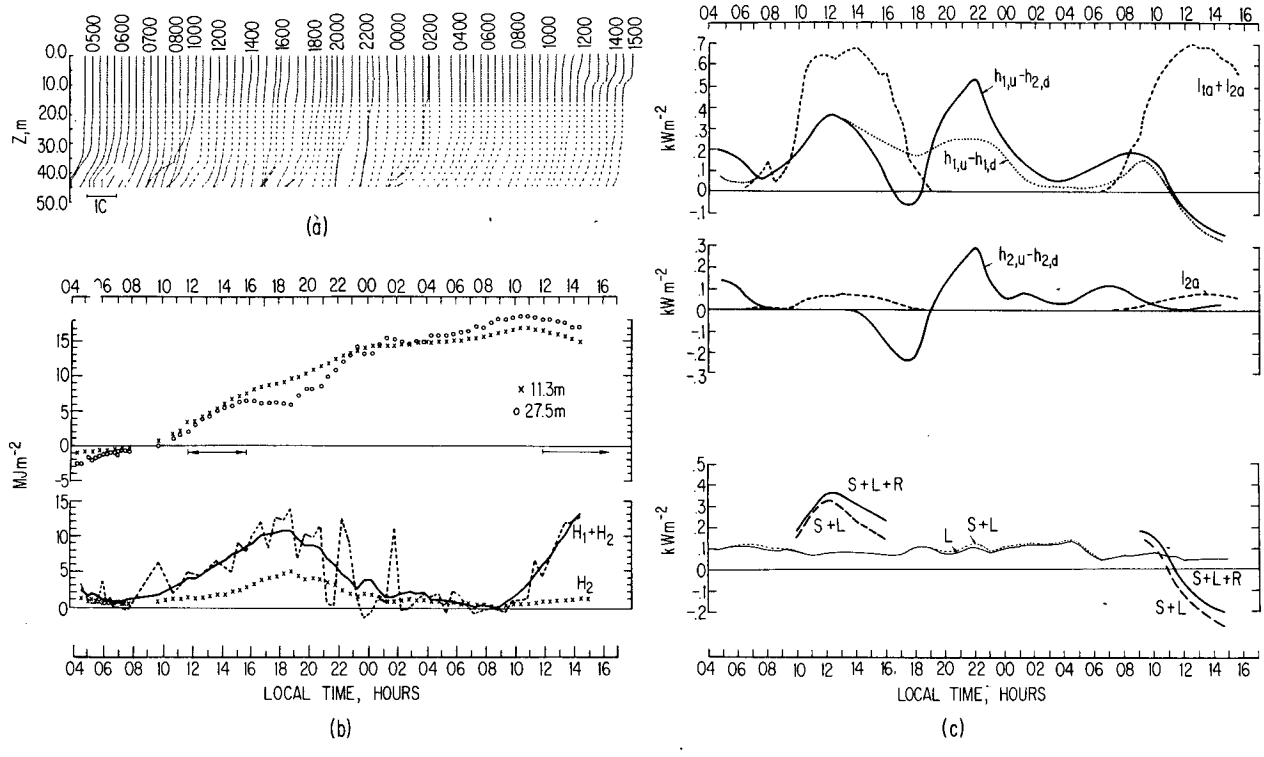

FIG. 7a. The set of temperature profiles for data set B. In this set a quasi-persistent interface appears at 11.3 m. 7b. The time-integrated heat content from the surface to 11.3 m (layer 1) and from the surface to 27.5 m (layer 1 and 2). $H_1 + H_2$ is the heat content from the surface to 27.5 m and H_2 is from 11.3 to 27.5 m. The solid line is smoothed. 7c. The various components of the heat balances of the two layers which occur. The symbols are the same as in Fig. 5. The surface fluxes as for Fig. 5. The fluxes $S + L + R$ and $S + L$ from the heat balance (heavy lines) are calculated only when sufficient layering is present to ensure they represent surface fluxes; the bulk formulas are shown by the faint lines.

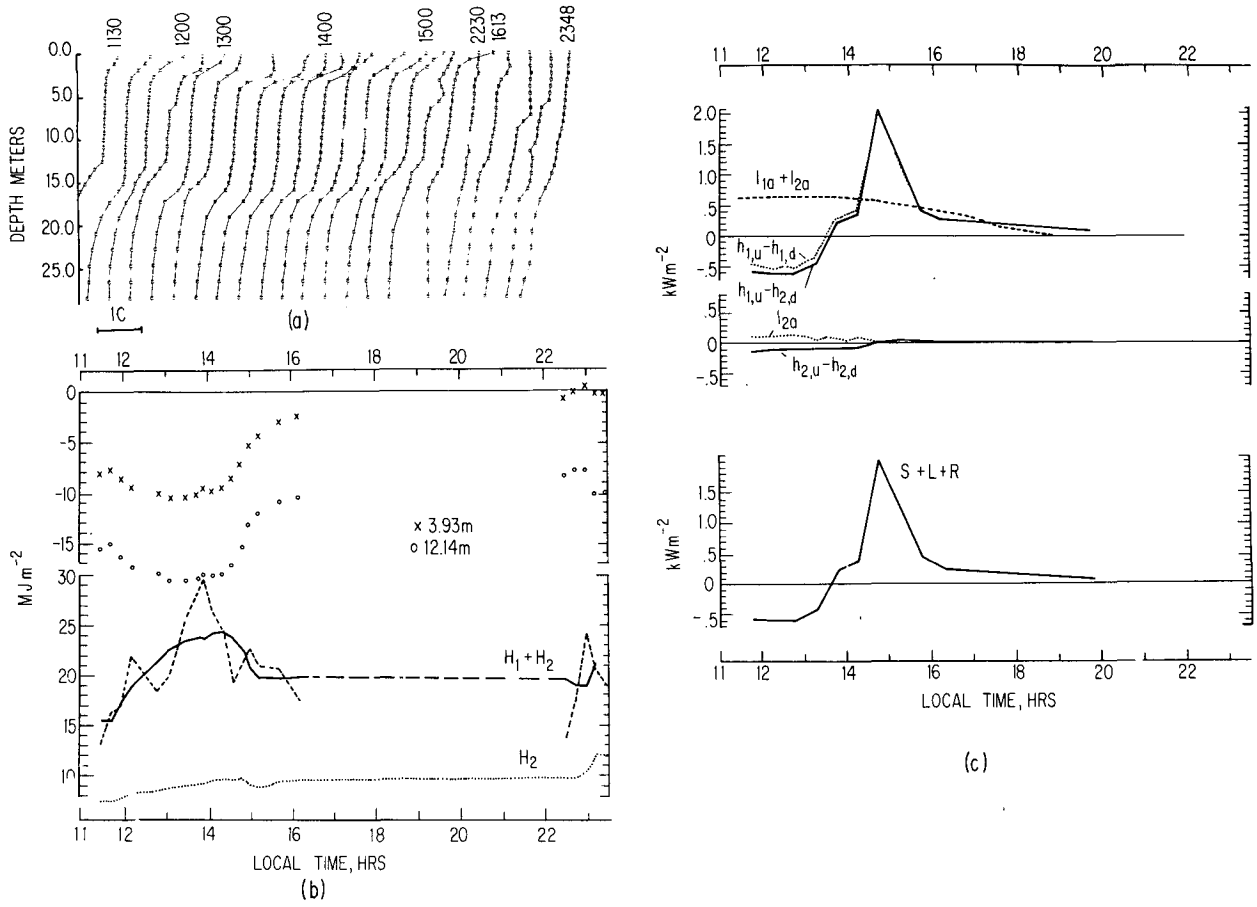

FIG. 8a. The set of temperature profiles for set C. Two mixed layers are evident; layer 1 from the surface to 3.93 and layer 2 from 3.93 to 12.14 m. 8b. The time-integrated heat content for layer 1 and layer 1 plus 2. $H_1 + H_2$ is the heat content for layer 1 and 2 and H_2 is for layer 2. 8c. The various components of the heat balance as in Fig. 5. Here $S + L + R$ is from the heat balance.

insolation absorbed in the upper two layers. The bottom curves represent the total heat flux and radiation absorption of the second or lower layer.

The average heat flux from the lower layer is less than 10% of that from the upper two layers; thus $h_{1,u} - h_{1,d}$ or $h_{1,u} - h_{2,d}$ is an adequate representation of the flux from the upper layer. This is taken as strong evidence that there is essentially no vertical heat flux across the 7.14 m interface. Looking at the H_i^* data, the slope of the 3.14 m data is the same as the other two indicating all the flux of heat out of the ocean comes from this layer; thus there is *no* flux across its bottom interface either.

The lower portion of Fig. 5c shows the measured and calculated surface fluxes for set A. The quantities S, L and R are, respectively, the sensible, latent and net longwave radiative components of the surface heat flux. If it is assumed all the heat flux out of the uppermost layer goes through the top surface, then $h_{1,a} - h_{1,d} = S + L + R$. This is justifiable because of the presence of the layers and because the horizontal heat transport is very small as is discussed above. Since R was measured with a net radiometer, $S + L$ could be determined from the heat content measurements also.

The broken curves $S + L$ and L were calculated from expressions given by Friehe and Schmidt (1976) from an examination of all flux data; in mks units (W m^{-2}) they are given by

$$S = 2.01 + 0.977 U \Delta T_1, \quad L = 5.32 U \Delta T_2, \quad (12)$$

where $\Delta T_1 = T_w - T_A$ and $\Delta T_2 = T_w - T_D$; T_A is air temperature, T_D dewpoint and T_w water temperature. Here ΔT_2 is used instead of a specific humidity difference since ΔT_2 over a limited temperature range is proportional to the specific humidity difference between the water surface and at 10 m.

Except for the period from 0200 to 1000, the bulk formulas grossly underestimate the heat fluxes determined from the heat content measurements. Throughout the measurement period $U \leq 3$ m s^{-1}.

The temperature profiles from set B are shown in Fig. 6a. This particular data set extends 36 h from before sunrise on 7 September to midafternoon on

8 September. During the first day, weak layering appears in the afternoon at a somewhat indeterminate depth of which is taken as 11.3 m. A more pronounced layer appears on the afternoon of the second day at that same depth. Before sunrise of each day, however, the thermal signatures of the layers are obliterated although the turbulent kinetic energy interface may still exist. Fig. 7 is the temperature at 0.4, 13.4 and 20.9 m for both days; 0.4 m is in the top layer while 13.4 and 20.9 m are in the lower layer. The time intervals and depths are indicated when definite interfaces can be recognized on the profiles. Even though layers cannot be distinguished at certain times the temperature differences at different levels indicate stability in the upper 21 m of water over longer intervals.

Fig. 6b gives the heat contents of the two layers of set B. The topmost layer (layer 1) extends down to 11.3 m and the lower layer (layer 2) from 11.3 m to 27.5 m. The heat balance terms for layer 1 and 2 are in Fig. 6c. The net heat flux from layer 2, $h_{2,u} - h_{2,d}$, is small from 0800–1500 on 8 September and on 9 September; from 1400 on 8 September to 0000 on 9 September relatively large heat flows to or from layer 2 occur. During most of this latter period there is no pronounced interface between layers 1 and 2, although a weak one was identifiable until 1600 on 8 September. During a significant portion of the time when the interlayer exchanges of heat are small, no interface is recognizable; however, no large exchanges of heat occur when a definite interface exists. The flux of heat out of layer 2 from 2000 on 8 September to about 0900 on 9 September appears to be during a period of lack of stability in the water as Fig. 7 indicates. The period from 1500–1900 on 8 September when layer 2 is being warmed (as well as up to 0400 on 9 September) is when large thermal anomalies were encountered and the heat content during this period is strongly contaminated by these anomalies. The interest, however, is on the periods when layers exist.

The surface fluxes, S, L and R, as measured from layer 1 and calculated from the bulk formulas, are also shown in Fig. 6c. The surface fluxes are only calculated when there is definite layering.

Data set C is quite limited in time but a very interesting situation occurred then. This was a day when the winds were calm and the sea generally glassy over 50% of its extent. A pronounced layer became evident at 3.9 m just before noon which was well over 1°C warmer than the water below. A second quite pronounced layer was evident throughout the period at 12.1 m. The profiles are given in Fig. 8a.

The various heat contents for set C are shown in Fig. 8b and the components of the heat balance in Fig. 8c. Large fluxes occur from layer 1 (0–3.9 m) and essentially zero fluxes from layer 2 (3.9–12.1 m). At about 1500 a rate of cooling of 2.09 kW m^{-2} was measured; however, this extreme rate appears to have occurred only over a 30 min interval. The heat loss rate of the upper 12 m of the ocean averaged over 9½ h was 0.272 kW m^{-2}, which is not excessive.

TABLE 2. Interface stabilities.

Data set	Layer depth (m)	$\partial T/\partial z$ (°C m^{-1})	Ri	h_{cond} (W m^{-2})
A	3.14	3.5×10^{-3}	8.8	2.1
	17.14	2.2	5.5	1.3
B	11.3	0.9	1.8	0.5
C	3.93	10.6	26.2	6.2
	12.14	3.5	8.8	2.1
Bruce and Firing (1974)	2	28.0	70	16.4

6. Stability of interfaces

When layers form which have density interfaces, turbulent mixing across them is governed by a Richardson number, as given in (4). Since stability of stratified shear flows appropriate to the ocean predicts that Ri > ¼ is a sufficient condition for stability of such a layer (Phillips, 1969), one would expect little or no turbulent heat transport across the observed interfaces when Ri > ¼. Convective transports will be zero because the salinity does not change across the interface and $\partial\rho/\partial z > 0$. Thermal *conductive* transports do occur but are small (for sea water the thermal conductivity is 1.3×10^{-3} cm^2 s^{-1}). For these layers, N can easily be determined from our profiles but we did not measure shear. In fact, virtually no data are available on shear values in the mixed layer. Simpson (1975) reports shear measurements in the Mediterranean outflow region. The largest small-scale value of shear they find is 4×10^{-2} s^{-1} closest to the mouth of the Mediterranean. In this region high shears would be expected. When pronounced shallow layering of the upper ocean occurs, the wind is usually light which suggests a very small shear across the density interface. For the data here a shear of 10^{-2} s^{-1} was used, probably a gross overestimate. The Ri values for the various layers and days are tabulated in Table 2. Except for set B, Ri $\gg$ ¼ implying no turbulent heat flux. In set B, Ri > ¼ but it certainly could become small enough on an intermittent basis to allow turbulent mixing as appeared to occur at times for set B.

The maximum heat fluxes h_{cond} (based on thermal conduction) which would occur are also given in

Table 2. The largest is 6.2 W m^{-2} compared to a surface flux of 2 kW m^{-2}.

The values of Ri were determined from the original data traces because the smoothing process used to display the data blurred over gradient maxima. The temperature gradient was the largest observed in a given profile and represents a typical value for the layer when well formed. For set B, the layer is not well formed and Ri varies from about ½ up to 3.

7. Large fluxes under calm winds

Data set C, taken when calm winds and high air temperatures predominated, shows extremely large heat fluxes. Set A also shows large fluxes in the afternoon, with some negative fluxes in the earlier part of the day. A similar situation was observed by Bruce and Firing (1974) in the same general area as our measurements in May 1973. "On a windless noticeably hot day with clear sky throughout the experiment, glassy sea surface, ..." they observed a surface layer of just over 1 m thick being about 3°C warmer than the underlying water; this was at 1840. A second profile was taken 2¾ h later; the warm surface layer was virtually gone. In this time period the upper 2 m of water cooled at a rate of 2.68 kW m^{-2}, and the next 5 m at a rate of 0.73 kW m^{-2}. The initial profile indicated a weaker interface of about 0.25°C at 7 m, and their data show no warming of the water below 7 m from 1800 to 2045. These several cases suggest that when conditions prevail under which pronounced shallow surface thermal layers form, anomalously large fluxes of heat from the ocean can occur.

8. Extreme points

An interesting check on the data, and a factor of possible significance in the determination of fluxes from heat balance measurements, is that usually twice per day the heat content of a layer or of the total mixed layer has an extremum in time. When this occurs $\partial H_i/\partial t$ in (2) is zero, and the total flux of heat out of the column of water under consideration is then equal to the rate of absorption in radiation. In most cases the heat content reaches a minimum somewhat after sunrise and in the late afternoon.

Looking back at data set A in Fig. 5b, $H_1 + H_2$ passes through a maximum somewhere before 1600, has a minimum at about 0700, and then a maximum about 1400 on the second day. The absorbed radiation and heat fluxes are in reasonably good agreement when the extrema occur. Table 3 presents all the extrema point data.

TABLE 3. Extrema points.

Set	Day	Time local	Nature	I_{abs} (W m^{-2})	$S+L+R$ (W m^{-2})
A	30 Aug	1600*	Max	>700	>700
	31 Aug	0700	Min	10	−20
	31 Aug	1400	Max	350–560	490
B	7 Sept	0700	Min	70	60
	7 Sept	1830	Max	60	60
	8 Sept	0900	Min	250	180
C	25 Aug	1415	Max	630	770
		1545	Min	450	420

* Extrema occurred just before this time.

9. Summary and conclusions

In this paper the heat budget of the upper 20 m of the ocean was examined for three periods when light to calm winds prevailed. Shallow surface layers were present which neither deepened nor became shallower in the mean. A total heat budget was determined in these cases and from the measurements the following conclusions are drawn:

1) The presence of statically stable layers at the ocean surface allows the determination of a heat budget without questions of vertical heat transports through the bottom or horizontal fluxes through the sides plaguing the interpretation of the results. The lighter the winds the smaller both fluxes become due to less mixing and weaker advection.

2) Time series of temperature data from the upper ocean measured from a slowly moving ship show much variability due to contamination from spatial inhomogeneities; however, by and large these can be removed from the data thus allowing a time representation of the temporal variation of the upper ocean. Short term (<2 h) variations can be removed by use of a running filter, which can be tuned to the dominant noise frequency. Longer term (layer spatial) variability which has persisted for times of a day or more can effectively be removed by subtracting a "reference" temperature measured below a stable density interface.

3) The presence of an extremum in the heat content, which usually occurs twice a day, allows a valuable check on the budget measurements. This feature might be valuable for estimating heat fluxes from the ocean since only radiation absorption need be determined at these times.

4) Under light wind conditions the bulk formulas for sensible and latent heat fluxes from the sea surface give values much less than those from the heat budget method employed here.

Other investigators from time to time have reported similar anomalies. The heat budget or heat content method is extremely simple and requires relatively unsophisticated equipment. It

needs much work to verify its validity but further investigations appear warranted because of its simplicity. It appears to work best where other methods have their greatest weakness—in light to calm winds. It is primarily of value to ocean heat flux studies since it measures the sum of L, S and R, whereas meteorologists need each component separately. Unless heat transports by mixed layer currents can be accurately determined, however, the heat content method is best applied to areas such as mid-ocean gyres where currents are weak and large-scale horizontal temperature gradients are small.

Acknowledgments. The author would like to thank Robert Hill for providing the surface irradiance and environmental data, and Dr. John Bergin for programming assistance. He also thanks the crew aboard the USNS *Lynch*.

REFERENCES

Bowden, K. F., M. R. Howe, and R. I. Tait, 1970: A study of the heat budget over a seven-day period at an oceanic station. *Deep-Sea Res.*, **17**, 401–411.

Bruce, J. G., and E. Firing, 1974: Temperature measurements in the upper 10 m with modified expendable bathythermograph probes. *J. Geophys. Res.*, **79**, 4110–4111.

Delnore, V. E., 1972: Diurnal variation of temperature and energy budget for the oceanic mixed layer during BOMEX. *J. Phys. Oceanogr.*, **2**, 239–247.

Friehe, C. A., and K. F. Schmitt, 1976: Parameterizations of air-sea interface fluxes of sensible heat and moisture by the bulk aerodynamic formulas. *J. Phys. Oceanogr.*, **6**, 801–809.

Jerlov, N. G., 1968: *Physical Oceanography*. Elsevier, 194 pp.

Halpern, D., and R. K. Reed, 1976: Heat budget of the upper ocean under light winds. *J. Phys. Oceanogr.*, **6**, 972–975.

Kaiser, J. A. C., 1976: The use of pyranometers for underwater total radiant energy flux measurements. *Deep-Sea Res.*, **23**, 881–887.

——, and K. G. Williams, 1974: Measurements of the vertical heat flux in the upper ocean layer. *J. Phys. Oceanogr.*, **4**, 137–144.

Payne, R. E., 1972: Albedo of the sea surface. *J. Atmos. Sci.*, **29**, 959–970.

Phillips, O. M., 1969: *The Dynamics of the Upper Ocean*. Cambridge University Press, 261 pp.

Shonting, D. H., 1964: Some observations of short-term heat transfer through the surface layers of the ocean. *Limnol. Oceanogr.*, **9**, 576–588.

Simpson, J. H., 1975: Observations of small scale vertical shear in the ocean. *Deep-Sea Res.*, **72**, 619–627.

Stommel, H., H. Saunders, W. Simmons, and J. Cooper, 1969: Observations of the diurnal thermocline. *Deep-Sea Res.*, **16**(suppl), 269–284.

——, and A. H. Woodcock, 1951: Diurnal heating of the surface of the Gulf of Mexico in the spring of 1942. *Trans. Amer. Geophys. Union*, **32**, 565–571.

Sverdrup, H. U., 1940: On the annual and diurnal variation of the evaporation from the oceans. *J. Mar. Res.*, **2**, 93–103.

U.S. Naval Oceanographic Office, 1965: *Oceanographic Atlas of the North Atlantic Ocean*. Section I. Tides and Currents. Naval Oceanográphic N.O. Publ. 700, Washington, D.C. 20390.

——, 1974: *The Gulf Stream*, **9**, No. 8.

Wyrtki, K., L. Magaard, and J. Hager, 1976: Eddy energy in the oceans. *J. Geophys. Res.*, **81**, 2641–2646.